

Article

Atmospheric Temperature and CO₂: Hen-Or-Egg Causality? (Version 1)

Demetris Koutsoyiannis ^{1,*}  and Zbigniew W. Kundzewicz ²

¹ Department of Water Resources and Environmental Engineering, School of Civil Engineering, National Technical University of Athens, 157 80 Athens, Greece

² Institute for Agricultural and Forest Environment, Polish Academy of Sciences, 60-809 Poznań, Poland; kundzewicz@yahoo.com or zkundze@man.poznan.pl

* Correspondence: dk@itia.ntua.gr

Received: 7 September 2020; Accepted: 11 September 2020; Published: 14 September 2020



Abstract: It is common knowledge that increasing CO₂ concentration plays a major role in enhancement of the greenhouse effect and contributes to global warming. The purpose of this study is to complement the conventional and established theory that increased CO₂ concentration due to human emissions causes an increase of temperature, by considering the reverse causality. Since increased temperature causes an increase in CO₂ concentration, the relationship of atmospheric CO₂ and temperature may qualify as belonging to the category of “hen-or-egg” problems, where it is not always clear which of two interrelated events is the cause and which the effect. We examine the relationship of global temperature and atmospheric carbon dioxide concentration at the monthly time step, covering the time interval 1980–2019, in which reliable instrumental measurements are available. While both causality directions exist, the results of our study support the hypothesis that the dominant direction is $T \rightarrow \text{CO}_2$. Changes in CO₂ follow changes in T by about six months on a monthly scale, or about one year on an annual scale. We attempt to interpret this mechanism by involving biochemical reactions, as at higher temperatures soil respiration, and hence CO₂ emission, are increasing.

Keywords: temperature; global warming; greenhouse gases; atmospheric CO₂ concentration

Πότερον ἡ ὄρνις πρότερον ἢ τὸ ᾠόν ἐγένετο (Which of the two came first, the hen or the egg?).

Πλούταρχος, *Ηθικά, Συμποσιακά Β, Πρόβλημα Γ* (Plutarch, *Moralia, Quaestiones convivales, B, Question III*).

1. Introduction

The phrase “hen-or-egg” is a metaphor describing situations where it is not clear which of two interrelated events or processes is the cause and which the effect. Plutarch was the first to pose this type of causality as a philosophical problem using the example of the hen and the egg, as indicated in the motto above. We note that in the original Greek text “ἡ ὄρνις” is feminine (article and noun) meaning the hen, rather than the chicken. Therefore, here we preferred the form “hen-or-egg” over “chicken-or-egg”, which is more common in English. (Very often, in online Greek texts, e.g., https://el.wikisource.org/wiki/Συμποσιακά_Β, “ἡ ὄρνις” appears as “ἡ ἄρνις”. After extended search, we contend that this must be an error, either an old one in manuscript copying, e.g., by monks in monasteries, or a modern one, e.g., in OCR. We are confident that the correct word is “ὄρνις”).

The objective of the paper is to demonstrate that the relationship of atmospheric CO₂ and temperature may qualify as belonging to the category of “hen-or-egg” problems. First, we discuss the relationship between temperature and CO₂ concentration by revisiting intriguing results from proxy data-based palaeoclimatic studies, where change in temperature leads and change in CO₂ concentration follows. Next, we discuss the data bases of modern (instrumental) measurements, related to global temperature and atmospheric CO₂ concentration, and introduce a methodology to analyse them. We develop a stochastic framework, introducing useful notions of time irreversibility and system causality, while we discuss the logical and technical complications in identifying causality, which prompt us to seek just necessary, rather than sufficient, causality conditions. In the Results section, we examine the relationship of these two quantities using the modern data, available at the monthly time step. We juxtapose time series of global temperature and atmospheric CO₂ concentration from several sources, covering the common time interval 1980–2019. In our methodology, it is the timing, rather than the magnitude, of changes that is important, being the determinant of causality. While logical, physically based arguments support the “hen-or-egg” hypothesis, indicating that both causality directions exist, interpretation of cross-correlations of time series of global temperature and atmospheric CO₂ suggests that the dominant direction is $T \rightarrow \text{CO}_2$, i.e., change in temperature leads and change in CO₂ concentration follows. We attempt to interpret this latter mechanism by noting the positive feedback loop—higher temperatures increase soil respiration and, hence, CO₂ emission.

The analysis reported in this paper was prompted by observation of an unexpected (and unfortunate) real-world experiment: during the Covid-19 lockdown in 2020, despite unprecedented decrease in carbon emission (Figure 1), there was increase in atmospheric CO₂ concentration, which followed a pattern similar to previous years (Figure 2). Indeed, according to the IEA [1], global CO₂ emissions were over 5% lower in the first quarter of 2020 than in that of 2019, mainly due to an 8% decline in emissions from coal, 4.5% from oil and 2.3% from natural gas. According to other estimates [2], the decrease is even higher: the daily global CO₂ emissions decreased by 17% by early April 2020 compared with the mean 2019 levels, while for the whole 2020 a decrease between 4% and 7% is predicted. Despite that, as seen in Figure 2, the normal pattern of atmospheric CO₂ concentration (increase until May and decrease in June and July) did not change. Similar was the behaviour after the 2008–2009 financial crisis, but the most recent situation is more characteristic because the Covid-19 decline in 2020 is the severest ever, including those in the world wars. It is also noteworthy in Figure 1 that there were three years in sequel without major increase in 2010s, where again there was increase in CO₂ concentration. (At first glance, this does not sound reasonable and therefore we have cross-checked the data with other sources, namely the Global Carbon Atlas, <http://www.globalcarbonatlas.org/en/CO2-emissions> and the data base of Our World In Data, <https://ourworldindata.org/grapher/annual-co-emissions-by-region>; we found only slight differences.) Interestingly, Figure 2 also shows a rapid growth in emissions after the 2008–2009 global financial crisis, which agrees with Peters et al. [3].

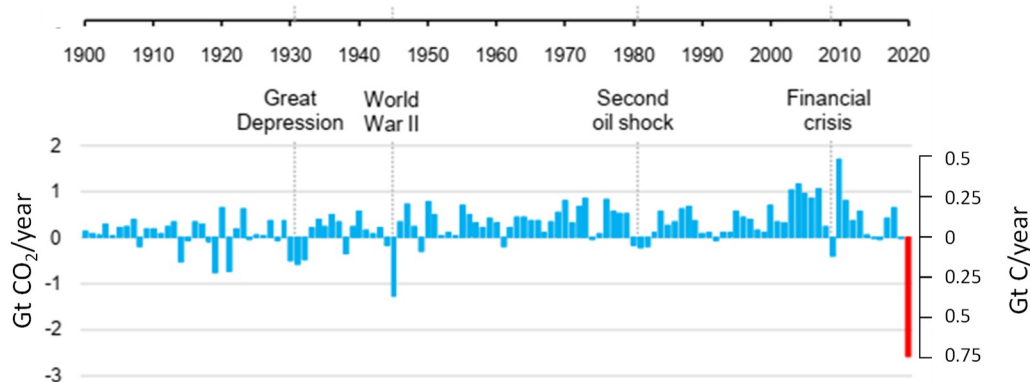


Figure 1. Annual change in global energy-related CO₂ emissions (adapted from IEA [1]).

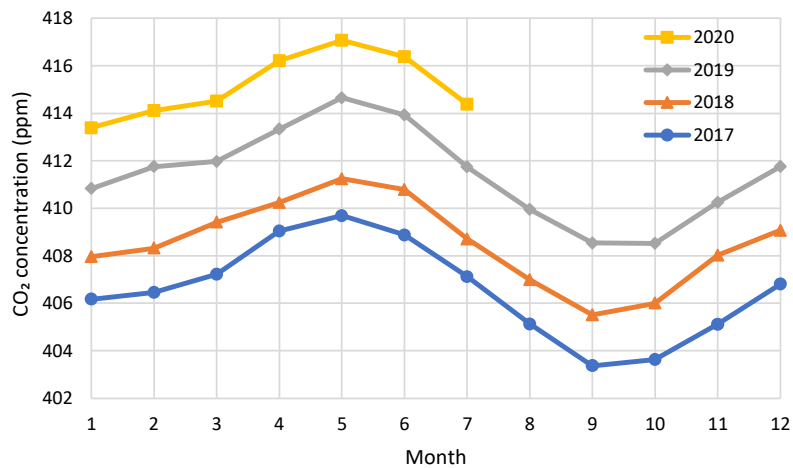


Figure 2. Atmospheric CO₂ concentration measured in Mauna Loa, Hawaii, USA, in the last four years.

2. Temperature and Carbon Dioxide—From Arrhenius and Palaeo-Proxies to Instrumental Data

Does the relationship of atmospheric carbon dioxide (CO₂) and temperature classify as a “hen-or-egg” type causality? If we look at the first steps of studying the link between the two, the reply is clearly negative. Arrhenius (1896, [4]), the most renowned scientist who studied the causal relationship between the two quantities, regarded the changes of the atmospheric carbon dioxide concentration as the cause and the changes of the temperature as the effect. Specifically, he stated:

Conversations with my friend and colleague Professor Högbom together with the discussions above referred to, led me to make a preliminary estimate of the probable effect of a variation of the atmospheric carbonic acid [meant CO₂] on the temperature of the earth. As this estimation led to the belief that one might in this way probably find an explanation for temperature variations of 5–10 °C, I worked out the calculation more in detail and lay it now before the public and the critics.

Furthermore, following the Italian meteorologist De Marchi (1895, [5]), whom he cited, he rejected what we call today *Milanković cycles* as possible causes of the glacial periods. In addition, he substantially overestimated the role of CO₂ in the greenhouse effect of the Earth’s atmosphere. He calculated the relative weights of absorption of CO₂ and water vapour as 1.5 and 0.88, respectively, a ratio of 1:0.6.

Arrhenius [4] also stated that “if the quantity of carbonic acid increases in geometric progression, the augmentation of the temperature will increase nearly in arithmetic progression”. This Arrhenius’s “rule” (which is still in use today) is mathematically expressed as:

$$T - T_0 = \alpha \ln\left(\frac{[\text{CO}_2]}{[\text{CO}_2]_0}\right) \tag{1}$$

where T and $[\text{CO}_2]$ denote temperature and CO₂ concentration, respectively, T_0 and $[\text{CO}_2]_0$ represent reference states, and α is a constant.

Here it is useful to note that Arrhenius’s studies were not the first on the subject. Arrhenius [4] cites several other authors, among whom Tyndall (1865, [6]) for pointing out the enormous importance of atmospheric absorption of radiation and for having the opinion that water vapour has the greatest influence on it. However, it appears that the first experiments on the subject, for both water vapour and carbon dioxide, were undertaken even earlier by the female scientist Eunice Newton Foote (1856, [7]; see also [8,9]).

While the fact that the two variables are tightly connected is beyond doubt, the direction of the simple causal relationship needs to be studied further. Today additional knowledge has been accumulated, particularly from palaeoclimatic studies, which allow us to examine Arrhenius’s hypotheses on a sounder basis. In brief, we can state the following:

- Indeed, CO₂ plays a substantial role as a greenhouse gas. However, modern estimates of the CO₂ contribution to the greenhouse effect largely differ from Arrhenius’s results, attributing 19% of the long-wave radiation absorption to CO₂ against 75% of water vapour and clouds (Schmidt et al., [10]), a ratio of 1:4.
- During the Phanerozoic Eon, Earth’s temperature has varied by even more than 5–10 °C, which was postulated by Arrhenius—see Figure 3. The link of temperature and CO₂ is beyond doubt, even though it is not clear in Figure 3, where it is seen that the CO₂ concentration has varied by about two orders of magnitude and does not always synchronize with the temperature variation. The relationship becomes more legible in proxy data of the Quaternary (see Figure 4). It has been demonstrated in a persuasive manner by Roe [11] that in the Quaternary it is the effect of Milanković cycles (variations in eccentricity, axial tilt, and precession of Earth’s orbit), rather than of atmospheric CO₂ concentration, that explains the glaciation process. Specifically (quoting Roe [11]),

variations in atmospheric CO₂ appear to lag the rate of change of global ice volume. This implies only a secondary role for CO₂—variations in which produce a weaker radiative forcing than the orbitally-induced changes in summertime insolation—in driving changes in global ice volume.

Despite falsification of some of Arrhenius’s hypotheses, his line of thought remained dominant. Yet there have been some important studies, based on palaeoclimatological reconstructions (mostly the Vostok ice cores [12,13]), which have pointed to the opposite direction of causality, i.e., the change of temperature as the cause and that in the CO₂ concentration as the effect. Such claims have explained the fact that temperature change leads and CO₂ concentration change follows. In agreement with Roe [11], several papers have found the time lag positive, with estimates varying from 50 to 1000 years, depending on the time period and the particular study [14–18]. Claims that CO₂ concentration leads (i.e., a negative lag) have not been generally made in these studies. At most a synchrony claim has been sought, on the basis that the estimated positive lags are often within the 95% uncertainty range [18] while in one of them [16] it has been asserted that a “short lead of CO₂ over temperature cannot be excluded”.

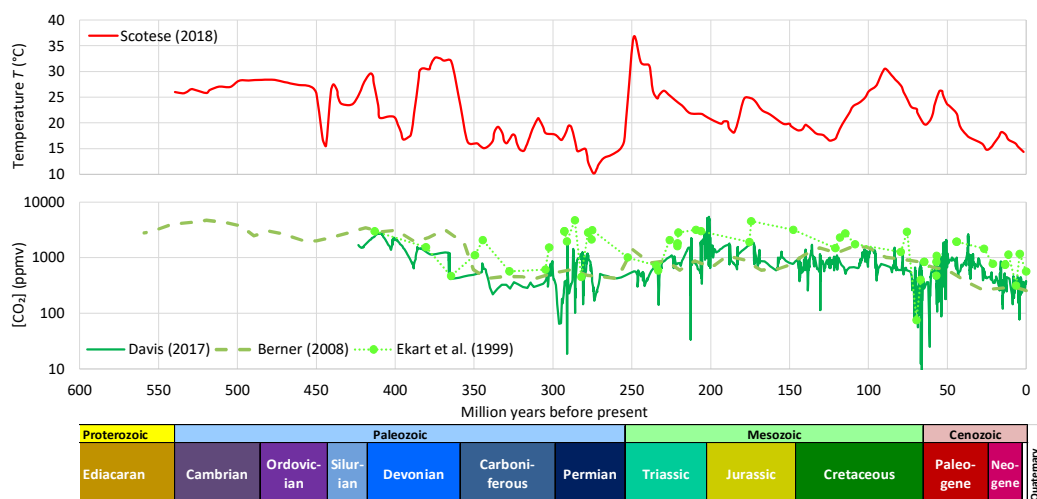


Figure 3. Proxy-based reconstructions of global mean temperature and CO₂ concentration during the Phanerozoic Eon. The temperature reconstruction by Scotese [19] was mainly based on proxies from [20–22], while the CO₂ concentration proxies have been taken from Davis [23], Berner [24] and Ekart et al. [25]; all original figures were digitized in this study. The chronologies of geologic eras shown in the bottom of the figure have been taken from the International Commission on Stratigraphy (<https://stratigraphy.org/chart>).

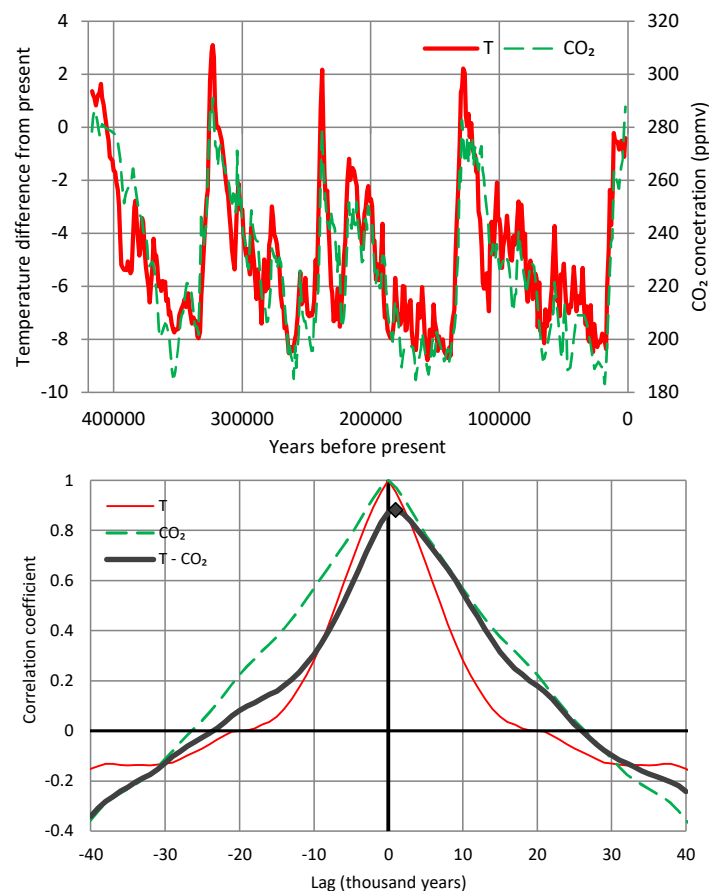


Figure 4. (upper) Time series of temperature and CO₂ concentration from the Vostok ice core, covering part of the Quaternary (420,000 years) with time step of 1000 years. (lower) Auto- and cross-correlograms of the two time series. The maximum value of the cross-correlation coefficient, marked as \blacklozenge , is 0.88 and appears at lag 1 (thousand years) (adapted from Koutsoyiannis [17]).

Since palaeoclimatic data suggest a direction opposite to that assumed by Arrhenius, Koutsoyiannis [17], using palaeoclimatic data from the Vostok ice cores at a time resolution of 1000 years and a stochastic framework similar to that of the present study (see Section 4.1) concluded that change in temperature precedes that of CO₂ by one time step (1000 years), as illustrated in Figure 4. He also noted that this causality condition holds for a wide range of time lags, up to 26,000 years, and hence the time lag is positive and most likely real. He asserted that the problem is obviously more complex than that of exclusive roles of cause and effect, classifying it in the “hen-or-egg” causality problems. Obviously, however, the proxy character of these data and the too-large time step of the time series reduce the reliability and accuracy of the results.

Studies exploring the rich body of modern datasets have also been published. Most of the studies have been based on the so-called “Granger causality test” (see Section 4.2). To mention a few, Kodra et al. [26] after testing several combinations and lags within the Granger framework, did not find any statistically significant results at the usual 5% significance level (they only found 2 cases at the 10% significance level; see their Tables 2 and 3). Stern and Kaufmann [27] studied, again within the Granger framework, the causality between radiative forcing and temperature and found that both natural and anthropogenic forcings cause temperature change, and also that the inverse is true, i.e., temperature causes greenhouse gas concentration changes. They concluded that their results

show that properly specified tests of Ganger causality validate the consensus that human activity is partially responsible for the observed rise in global temperature and that this rise in temperature also has an effect on the global carbon cycle.

In contrast, Stips et al. [28] used a different method [29] to investigate the causal structure and concluded that their

study unambiguously shows one-way causality between the total Greenhouse Gases and GMTA [global mean surface temperature anomalies]. Specifically, it is confirmed that the former, especially CO₂, are the main causal drivers of the recent warming.

Here we use a different path to study the causal relation between temperature and CO₂ concentration with the emphasis given on the exploratory and explanatory aspect of our analyses. While we occasionally use the Ganger statistical test, this is not central in our approach. Rather, we give the emphasis on time directionality in the relationship, which we try to identify in the simplest possible manner, i.e., by finding the lag, positive or negative, which maximizes the cross-correlation between the two processes (see Section 4.1). We visualize our results by plots, so as to be simple, transparent, intuitive, readily understandable by the reader and hopefully persuading. For the algorithmic-friendly reader we also provide statistical testing results which just confirm what is directly seen in the graphs.

Another difference of our study from most of the earlier ones is our focus on changes, rather than current states, in the processes we investigate. This puts in central place in our analyses the technique of process differencing. This technique is quite natural and also powerful in studying time directionality [17]. We note that differencing (which has also been used in Reference [26]) has been criticized for potentially eliminating long-run effects and hence providing information on short-run effects only [27]. Even if this speculation were valid, it would not invalidate the differencing technique for the following reasons:

- The short-run effects deserve to be studied, as well as the long-term ones.
- The modern instrumental records are short themselves and only allow the short-term effects to be studied.
- For the long-term effects, the palaeo-proxies provide better indications, which have already been discussed above.

3. Data

Our investigation of the relationship of temperature and concentration of carbon dioxide in the atmosphere is based on two time series of the former process and four of the latter. Specifically, the temperature data are of two origins, satellite and ground based. The satellite dataset, developed at the University of Alabama in Huntsville (UAH), infers the temperature, T , of three broad levels of the atmosphere from satellite measurements of the oxygen radiance in the microwave band, using advanced (passive) microwave sounding units on NOAA and NASA satellites [30,31]. The data are publicly available on monthly scale in the forms of time series of “anomalies” (defined as differences from long-term means) for several parts of earth, as well as in maps. Here we use only the global average on monthly scale for the lowest level, referred to as the lower troposphere. The ground-based data series we use is the CRUTEM.4.6.0.0 global T2m land temperature [32]. This originates from a gridded dataset of historical near-surface air temperature anomalies over land. Data are available for each month from January 1850 to the present. The dataset is a collaborative product of the Met Office Hadley Centre and the Climatic Research Unit at the University of East Anglia. We note that both sources of information, UAH and CRUTEM, provide time series over the globe, land and oceans; here we deliberately use one source for the globe and one for the land.

The two temperature series used in the study are depicted in Figure 5. They are consistent with each other (and correlated, $r = 0.8$), yet the CRUTEM4 series shows a larger increasing trend than the UAH series. The differences are explainable by three reasons: (a) the UAH series includes both land and sea, while the chosen CRUTEM4 series is for land only, in which the increasing trend is substantially higher than in sea; (b) the UAH series refers to some high altitude in the troposphere (see details in Koutsoyiannis [33]), while the CRUTEM4 series refers to the ground level; and (c) the ground-based CRUTEM4 series is affected by urbanization (a lot of ground stations are located in

urban areas). In any case, the difference in the increasing trends is irrelevant for the current study, as the timing, rather than the magnitude, of changes is the determinant of causality. This will be manifest in our results.

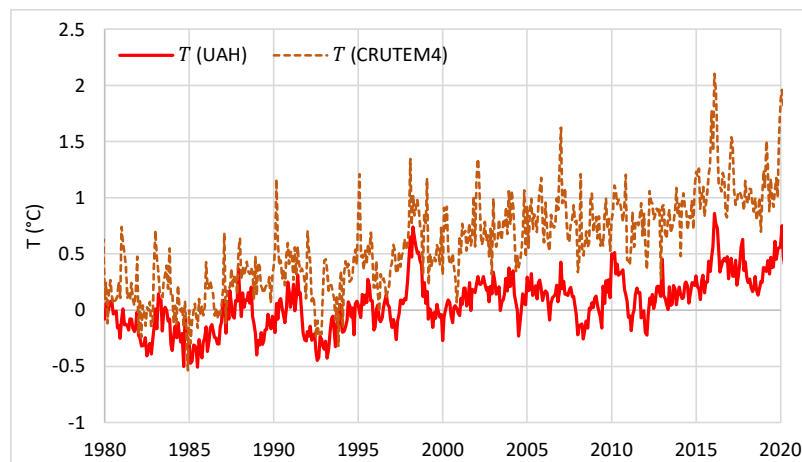


Figure 5. Plots of the data series of global temperature “anomalies” since 1980, as used in the study, from satellite measurements over the globe (UAH) and from ground measurements over land (CRUTEM4).

The most famous CO₂ dataset is that of Mauna Loa Observatory [34]. The Observatory, located on the north flank of Mauna Loa Volcano, on the Big Island of Hawaii, USA, at an elevation of 3397 m above sea level, is a premier atmospheric research facility that has been continuously monitoring and collecting data related to the atmosphere since the 1950s. The NOAA has also other stations that systematically measure atmospheric CO₂ concentration, namely at Barrow, Alaska, USA and at South Pole. The NOAA’s Global Monitoring Laboratory Carbon Cycle Group also computes global mean surface values of CO₂ concentration using measurements of weekly air samples from the Cooperative Global Air Sampling Network. The global estimate is based on measurements from a subset of network sites. Only sites where samples are predominantly of well-mixed marine boundary layer air, representative of a large volume of the atmosphere, are considered (typically at remote marine sea level locations with prevailing onshore winds). Measurements from sites at high altitude (such as Mauna Loa) and from sites close to anthropogenic and natural sources and sinks are excluded from the global estimate. (Details about this dataset are provided in https://www.esrl.noaa.gov/gmd/ccgg/about/global_means.html).

The period of data coverage varies, but all series cover the common 40-year period 1980–2019, which hence constituted the time reference of all our analyses. As a slight exception, the Barrow (Alaska) and South Pole measurements have not yet been available in final form for 2019 and, thus, this year was not included in our analyses of these two time series. The data of the latter two stations are given in irregular-step time series, which was regularized (by interpolation) to monthly in this study. All other data series have already been available on a monthly scale.

All four CO₂ time series used in the study are depicted in Figure 6. They show a superposition of increasing trends and annual cycles whose amplitudes increase as we head from the South to the North Pole. The South Pole series has opposite phase of oscillation compared to the other three.

The annual cycle is better seen in Figure 7, where we have removed the trend with standardization, namely by dividing each monthly value by the geometric average of the 5-year period before it. The reason why we used division rather than subtraction and geometric rather than arithmetic average (being thus equivalent to subtracting or averaging the logarithms of CO₂ concentration), will become evident in Section 5. In the right panel of Figure 7, which depicts monthly statistics of the time series of the left panel, it is seen that in all sites but the South Pole the annual maximum occurs in May; that of the South Pole occurs in September.

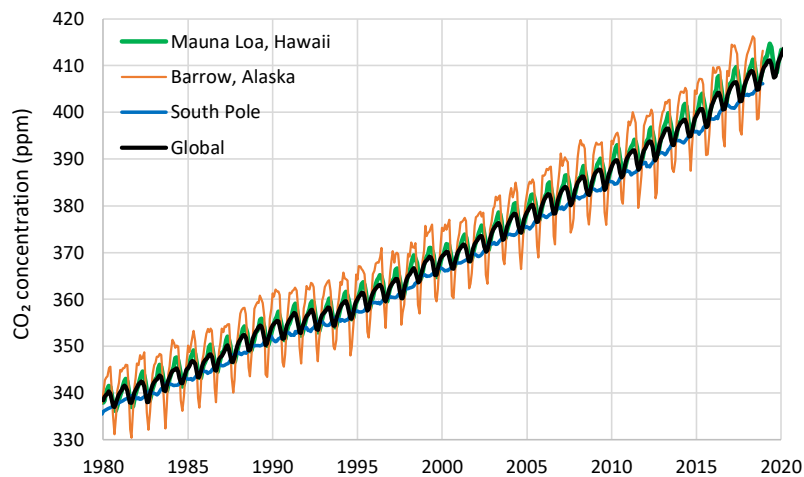


Figure 6. Plots of the data series of atmospheric CO₂ concentration measured in Mauna Loa (Hawaii, USA), Barrow (Alaska, USA) and South Pole, and global average.

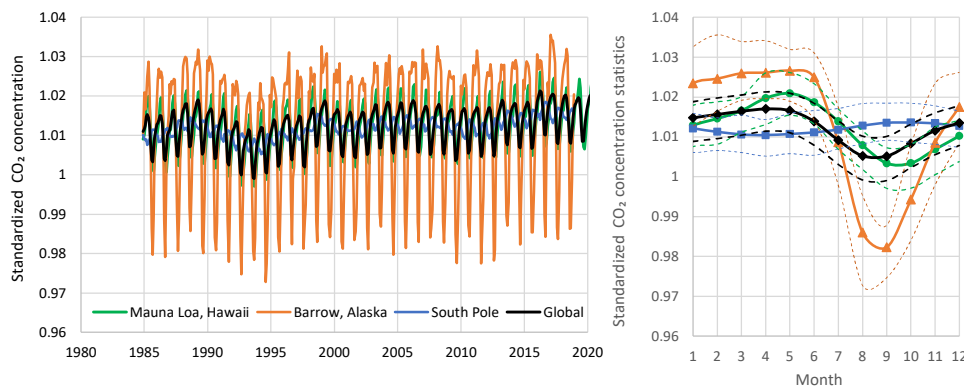


Figure 7. Plots of atmospheric CO₂ concentration after standardization: (left) each monthly value is standardized by dividing with the geometric average of the 5-year period before it. (right) Monthly statistics of the values of the left panel; for each month the average is shown in continuous line and the minimum and maximum in thin dashed lines of the same colour as the average.

4. Methods

4.1. Stochastic Framework

A recent study [17] has investigated time irreversibility in hydrometeorological processes and developed a theoretical framework in stochastic terms. It also studied necessary conditions for causality, which is tightly linked to time irreversibility. A simple definition of time reversibility within stochastics is the following, where underlined symbols denote stochastic (random) variables and non-underlined ones denote values thereof or regular variables.

A stochastic process $\underline{x}(t)$ at continuous time t , with n th order distribution function:

$$F(x_1, x_2, \dots, x_n; t_1, t_2, \dots, t_n) := P\{\underline{x}(t_1) \leq x_1, \underline{x}(t_2) \leq x_2, \dots, \underline{x}(t_n) \leq x_n\} \tag{2}$$

is time-symmetric or time-reversible if its joint distribution does not change after reflection of time about the origin, i.e., if for any n, t_1, t_2, \dots, t_n ,

$$F(x_1, x_2, \dots, x_n; t_1, t_2, \dots, t_n) = F(x_1, x_2, \dots, x_n; -t_1, -t_2, \dots, -t_n) \tag{3}$$

If times t_i are equidistant, i.e., $t_i - t_{i-1} = D$, the definition can be also written by reflecting the order of points in time, i.e.:

$$F(x_1, x_2, \dots, x_{n-1}, x_n; t_1, t_2, \dots, t_{n-1}, t_n) = F(x_1, x_2, \dots, x_{n-1}, x_n; t_n, t_{n-1}, \dots, t_2, t_1) \tag{4}$$

A process that is not time-reversible is called time-asymmetric, time-irreversible or time-directional. Important results related to time (ir)reversibility are the following:

- A time reversible process is also stationary (Lawrance [35]).
- If a scalar process $\underline{x}(t)$ is Gaussian (i.e., all its finite dimensional distributions are multivariate normal) then it is reversible (Weiss [36]). The consequences are: (a) a directional process cannot be Gaussian; (b) a discrete-time ARMA process (and a continuous-time Markov process) is reversible if and only if it is Gaussian.
- However, a vector (multivariate) process can be Gaussian and irreversible at the same time. A multivariate Gaussian linear process is reversible if and only if its autocovariance matrices are all symmetric (Tong and Zhang [37]).

Time asymmetry of a process can be studied more conveniently (or even exclusively in a scalar process) through the differenced process, i.e.:

$$\widetilde{\underline{x}}_{\tau,\nu} := \underline{x}_{\tau+\nu} - \underline{x}_{\tau} \tag{5}$$

for an appropriate time-step ν of differencing. The differenced process represents change of the original process within a time period of length ν . We further define the cumulative process of \underline{x}_{τ} for discrete time κ as:

$$\underline{X}_{\kappa} := \underline{x}_1 + \underline{x}_2 + \dots + \underline{x}_{\kappa} \tag{6}$$

Through this, we find that the time average of the original process \underline{x}_{τ} for discrete time scale κ is:

$$\underline{x}_{\tau}^{(\kappa)} := \frac{\underline{x}_{(\tau-1)\kappa+1} + \underline{x}_{(\tau-1)\kappa+2} + \dots + \underline{x}_{\tau\kappa}}{\kappa} = \frac{\underline{X}_{\tau\kappa} - \widetilde{\underline{X}}_{(\tau-1)\kappa}}{\kappa} \tag{7}$$

Similar equations for the cumulative and averaged processes for the differenced process $\widetilde{\underline{x}}_{\tau,\nu}$ are given in Appendix A.1.

The variance of the process $\underline{x}_{\tau}^{(\kappa)}$ is a function of the time scale κ which is termed the climacogram of the process:

$$\gamma_{\kappa} := \text{var} \left[\underline{x}_{\tau}^{(\kappa)} \right] \tag{8}$$

The autocovariance function for time lag η is derived from the climacogram through the relationship [38]:

$$c_{\eta} = \frac{(\eta + 1)^2 \gamma_{|\eta+1|} + (\eta - 1)^2 \gamma_{|\eta-1|}}{2} - \eta^2 \gamma_{|\eta|} \tag{9}$$

For sufficiently large κ (theoretically as $\kappa \rightarrow \infty$), we may approximate the climacogram as:

$$\gamma_{\kappa} \propto \kappa^{2H-2} \tag{10}$$

where H is termed the *Hurst parameter*. The theoretical validity of such (power-type) behaviour of a process was implied by Kolmogorov (1940 [39]). The quantity $2H-2$ is visualized as the slope of the double logarithmic plot of the climacogram for large time scales. In a random process, $H = 1/2$, while in most natural processes $1/2 \leq H \leq 1$, as first observed by Hurst (1951 [40]). This natural behaviour is known as (long-term) *persistence* or *Hurst-Kolmogorov (HK) dynamics*. A high value of H (approaching 1) indicates enhanced presence of patterns, enhanced change and enhanced uncertainty

(e.g., in future predictions). A low value of H (approaching 0) indicates enhanced fluctuation or *antipersistence* (sometimes misnamed as quasi-periodicity, as the period is not constant).

For a stationary stochastic process \underline{x}_τ , the differenced process $\widetilde{\underline{x}}_\tau$ has mean zero and variance:

$$\widetilde{\gamma}_{v,1} := \text{var}[\widetilde{\underline{x}}_{\tau,\nu}] = \text{var}[\underline{x}_{\tau+\nu}] + \text{var}[\underline{x}_\tau] - 2\text{cov}[\underline{x}_{\tau+\nu}, \underline{x}_\tau] = 2(\gamma_1 - c_\nu) \tag{11}$$

where γ_1 and c_ν are the variance and lag ν autocovariance, respectively, of \underline{x}_τ . Furthermore, it has been demonstrated [17] that the Hurst coefficient of the differenced process $\widetilde{\underline{x}}_\tau$ precisely equals zero, which means that $\widetilde{\underline{x}}_\tau$ is completely antipersistent, irrespective of γ_κ .

In vector processes, to study irreversibility we can use second order moments, and in particular cross-covariances among the different components of the vector. In particular (adapting and simplifying the analyses and results in Koutsoyiannis, [17]), given two processes \underline{x}_τ and \underline{y}_τ we could study the cross-correlations:

$$r_{\widetilde{\underline{x}}\widetilde{\underline{y}}}[v, \eta] = \text{corr}[\widetilde{\underline{x}}_{\tau,\nu}, \widetilde{\underline{y}}_{\tau+\eta,\nu}] \tag{12}$$

Time (ir)reversibility could then be characterized by studying the properties of symmetry or asymmetry of $r_{\widetilde{\underline{x}}\widetilde{\underline{y}}}(v, \eta)$ as a function of the time lag η . In a symmetric bivariate process, $r_{\widetilde{\underline{x}}\widetilde{\underline{y}}}[v, \eta] = r_{\widetilde{\underline{x}}\widetilde{\underline{y}}}[v, -\eta]$ and if the two components are positively correlated, the maximum of $r_{\widetilde{\underline{x}}\widetilde{\underline{y}}}[v, \eta]$ will appear at lag $\eta = 0$. If the bivariate process is irreversible, this maximum will appear at a lag $\eta_1 \neq 0$ and its value will be $r_{\widetilde{\underline{x}}\widetilde{\underline{y}}}[v, \eta_1]$.

Time asymmetry is closely related to causality, which presupposes irreversibility. Thus, “no causal process (i.e., such that of two consecutive phases, one is always the cause of the other) can be reversible” (Heller, [41]; see also [42]). In probabilistic definitions of causality, time asymmetry is determinant. Thus, Suppes [43] defines causation thus: “An event $B_{t'}$ [occurring at time t'] is a prima facie cause of the event A_t [occurring at time t] if and only if (i) $t' < t$, (ii) $P\{B_{t'}\} > 0$, (iii) $P(A_t|B_{t'}) > P(A_t)$ ”. Also, Granger’s [44] first axiom in defining causality reads, “The past and present may cause the future, but the future cannot”.

Consequently, in simple causal systems, in which the process component \underline{x}_τ is the cause of \underline{y}_τ (like in the clear case of rainfall and runoff, respectively), it is reasonable to expect $r_{\widetilde{\underline{x}}\widetilde{\underline{y}}}[v, \eta] \geq 0$ for any $\eta \geq 0$, while $r_{\widetilde{\underline{x}}\widetilde{\underline{y}}}[v, \eta] = 0$ for any $\eta < 0$. However, in “hen-or-egg” causal systems, this will not be the case and we reasonably expect $r_{\widetilde{\underline{x}}\widetilde{\underline{y}}}[v, \eta] \neq 0$ for any η . Yet, we can define a dominant direction of causality based on the time lag η_1 maximizing cross-correlation. Formally, η_1 is defined for a specified v as:

$$\eta_1 := \underset{\eta}{\text{argmax}} |r_{\widetilde{\underline{x}}\widetilde{\underline{y}}}(v, \eta)| \tag{13}$$

We can thus distinguish the following three cases:

- If $\eta_1 = 0$ then there is no dominant direction.
- If $\eta_1 > 0$ then the dominant direction is $\underline{x}_\tau \rightarrow \underline{y}_\tau$.
- If $\eta_1 < 0$ then the dominant direction is $\underline{y}_\tau \rightarrow \underline{x}_\tau$.

Justification and further explanations on these conditions are provided in Appendix A.2.

4.2. Complications in Seeking Causality

It must be stressed that the above conditions are put as necessary and not sufficient conditions for a causative relationship between the processes \underline{x}_τ and \underline{y}_τ . Following Koutsoyiannis [17] (where additional necessary conditions are discussed), we avoid seeking sufficient conditions, a task that would be too difficult or impossible due to its deep philosophical complications as well as the logical and technical ones.

Specifically, it is widely known that correlation is not causation. As Granger [44] puts it,

when discussing the interpretation of a correlation coefficient or a regression, most textbooks warn that an observed relationship does not allow one to say anything about causation between the variables.

Perhaps that is the reason why Suppes [43] uses the term “prima facie cause” in his definition given above, which however he does not explain, apart for attributing “prima facie” to Jaakko Hintikka. Furthermore, Suppes discusses *spurious causes* and eventually defines the *genuine cause* as a “prima facie cause that is not spurious”; he also discusses the very existence of genuine causes which under certain conditions (e.g., in a Laplacean universe) seems doubtful.

Granger himself also uses the term “prima facie cause”, while Granger and Newbold [45] note that a cause satisfying a causality test still remains prima facie because it is always possible that, if a different information set were used, then it would fail the new test. Despite the caution issued by its pioneers, including Granger, through the years the term “Granger causality” has become popular (particularly in the so-called “Granger causality test”, e.g., [46]). Probably because of that misleading term, the technique is sometimes thought of as one that establishes causality, thus resolving or overcoming the “correlation is not causation” problem. In general, it has rarely been understood that identifying genuine causality is not a problem of choosing the best algorithm to establish a statistical relationship (including its directionality) between two variables. As an example of misrepresentation of the actual problems, see Reference [47], which contains the statement:

Determining true causality requires not only the establishment of a relationship between two variables, but also the far more difficult task of determining a direction of causality.

In essence, the “Granger causality test” studies the improvement of prediction of a process y_τ by considering the influence of a “causing” process x_τ through the Granger regression model:

$$y_\tau = \sum_{j=1}^{\eta} a_j y_{\tau-j} + \sum_{j=1}^{\eta} b_j x_{\tau-j} + \varepsilon_\tau \tag{14}$$

where a_j and b_j are the regression coefficients and ε_τ is an error term. The test is based on the null hypothesis that the process x_τ is not actually causing y_τ , formally expressed as:

$$H_0 : b_1 = b_2 = \dots = b_\eta = 0 \tag{15}$$

Algorithmic details of the test are given in Reference [46], among others. The rejection of the null hypothesis is commonly interpreted in the literature with a statement that x_τ “Granger-causes” y_τ .

This is clearly a misstatement and, in fact, the entire test is based on correlation matrices. Thus, it again reflects correlation, rather than causation. The rejection of the null hypothesis signifies improvement of prediction and this does not mean causation. To make this clearer, let us consider the following example: people sweat when the atmospheric temperature is high—and also wear light cloths. Thus, it is reasonably expected that in a prediction of sweat quantity temperature matters. In absence of temperature measurements (e.g., when we have only visual information, like when watching a video), algorithmically the weight of the cloths improves the prediction of the sweat quantity. But we could not say that the decrease of cloth weight causes increase of sweat (the opposite would be more reasonable and would most probably become evident in a three-variable regression, temperature – cloth weight – sweat).

Cohen [48] suggested replacing the term “Granger causality” with “Granger prediction” after correctly pointing out that:

Results from Granger causality analyses neither establish nor require causality. Granger causality results do not reveal causal interactions, although they can provide evidence in support of a hypothesis about causal interactions.

To avoid such philosophical and logical complications, here we replace the “prima facie” or “Granger” characterization of a cause and, as we already explained, we abandon seeking for genuine

causes, by using the notion of *necessary conditions* for causality. One could say that if two processes satisfy the necessary conditions, then they define a *prima facie* causality, but we avoid stressing that as we deem it unnecessary. Furthermore, we drop “causality” from “Granger causality test”, thus hereinafter calling it “Granger test”.

Some have thought they can approach genuine causes and get rid of the caution “correlation is not causation” by replacing the correlation with other statistics in the mathematical description of causality. For example, Liang [29] uses the concept of information (or entropy) flow (or transfer) between two processes; this method has been called “Liang causality” in the already cited work he co-authors [28]. The usefulness of such endeavours is not questioned yet their vanity to determine genuine causality is easy to infer: It suffices to consider the case where the two processes, for which causality is studied, are jointly Gaussian. It is well known that in any multivariate Gaussian process the covariance matrix (or the correlation matrix along with the variances) fully determines all properties of the multivariate distribution of any order. For example, the mutual information in a bivariate Gaussian process is (Papoulis, [49]):

$$H[y|x] = \ln \sigma_y \sqrt{2\pi e(1-r^2)} \quad (16)$$

where σ and r denote standard deviation and correlation, respectively. Thus, using any quantity related to entropy (equivalently, information), is virtually identical to using correlation. Furthermore, in Gaussian processes, whatever statistic is used in describing causality, it is readily reduced to correlation. This is evident even in Liang [29], where, e.g., in his Equation (102) the information flow turns out to be the correlation coefficient multiplied by a constant. In other words, the big philosophical problem of causality cannot be resolved by technical tricks.

From what was exposed above (Section 4.1), the time irreversibility and the time directionality is most important in seeking causality. In this respect, we certainly embrace Suppes’s condition (i) and Granger’s first axiom, as stated above. Furthermore, we believe there is no meaning in refusing that axiom and continuing to speak about causality. We note though that there have been recent attempts to show that

coupled chaotic dynamical systems violate the first principle of Granger causality that the cause precedes the effect. [50]

Apparently, however, the particular simulation experiment performed in the latter work, which, notably, is not even accompanied by any attempt for deduction based on stochastics, cannot show any violation. In our view, such a violation, if indeed happened, would be violation of logic and perhaps of common sense.

4.3. Additional Clarifications of Our Approach

After the above theoretical and methodological discourse, we can clarify our methodological approach by emphasizing the following points.

1. To make our assertions and, in particular, to use the “hen-or-egg” metaphor, we do not rely on merely statistical arguments. If we did that, based on our results presented in next section, we would conclude that only the causality direction $T \rightarrow [\text{CO}_2]$ exists. However, one may perform a thought experiment of instantly adding a big quantity of CO_2 to the atmosphere. Would the temperature not increase? We believe it would, as CO_2 is known to be a greenhouse gas. The causation in the opposite direction is also valid, as will be discussed in Section 6, “Physical interpretation”. Therefore, we assert that both causality directions exist and we are looking for the dominant one under the current climate conditions, those manifest in the datasets we use, instead of trying to make assertions of an exclusive causality direction.

2. While we occasionally use statistical tests (namely, the Granger test, Equations (14)–(15)), we opt to use as the central point of our analyses Equation (13) (and the conditions below it) because it is more intuitive and robust, it fully reflects the basic causality axiom of time precedence, and it is more straightforward, transparent (free of algorithmic manipulations) and easily reproducible (without a need for specialized software).
3. For simplicity, we do not use here any statistic other than correlation. We stress that the system we are examining indeed classifies as Gaussian and thus it is totally unnecessary to examine any statistic additional to correlation. The evidence of Gaussianity is provided by Figure A1 in Appendix A.3, in terms of marginal distributions of the processes examined, and in terms of their relationship. In particular, Figure A2 suggests a typical linear relationship for the bivariate process. We note that the linearity here is not a simplifying assumption or a coincidence, as there are theoretical reasons implying it, which are related to the principle of maximum entropy [49,51].
4. All in all, we adhere to simplicity and transparency and, in this respect, we illustrate our results graphically, so they are easily understandable, intuitive and persuasive. Indeed, our findings are easily verifiable even from simple synchronous plots of time series, yet we also include plots of autocorrelations and lagged cross-correlation, which are also most informative in terms of time directionality.

5. Results

5.1. Original Time Series

Here we examine the relationship of atmospheric temperature and carbon dioxide concentration using the modern data (observations rather than proxies), available at the monthly time step, as described in Section 3. To apply our stochastic framework, we must first make the two time series linearly compatible. Specifically, based on Arrhenius's rule (Equation (1)), we take the logarithms of CO₂ concentration, while we keep T untransformed. Such a transformation has been performed also in previous studies, which consider the logarithm of CO₂ concentration as a proxy of total radiative forcing (e.g., [26]). However, by calling this quantity "forcing" we indirectly give it a priori (i.e., before investigating causation) the role of the cause. Therefore, here we avoid such interpretations; we simply call this variable the logarithm of carbon dioxide concentration and denote it as $\ln[\text{CO}_2]$.

A synchronous plot of the two processes (specifically, UAH temperature and $\ln[\text{CO}_2]$ at Mauna Loa) is depicted in Figure 8. Very little can be inferred from this figure alone. Both processes show increasing trends and thus appear as positively correlated. On the other hand, the two processes appear to have different behaviours. Temperature shows an erratic behaviour while $\ln[\text{CO}_2]$ has a smooth evolution marked by the annual periodicity. It looks impossible to infer causality from that graph alone.

Somewhat more informative is Figure 9, based on the methodology in Section 4.1, by studying lagged cross-correlations of the two processes but without differencing the processes. Specifically, Figure 9 shows the cross-correlogram between UAH temperature and Mauna Loa $\ln[\text{CO}_2]$ at monthly and annual scales; the autocorrelograms of the two processes are also plotted for comparison. In both time scales the cross-correlogram shows high correlations at all lags, with the maximum attained at lag zero. This does give a hint about the direction. However, the cross-correlations for negative lags are slightly greater than those in the positive lags. Notice that to make this clearer, we have also plotted the differences $r_j - r_{-j}$ in the graph. This behaviour could be interpreted as supporting the causality direction $[\text{CO}_2] \rightarrow T$. However, we deem that the entire picture is spurious as it is heavily affected by the fact that the autocorrelations are very high and, in particular, those of $\ln[\text{CO}_2]$ are very close to 1 for all lags shown in the figure.

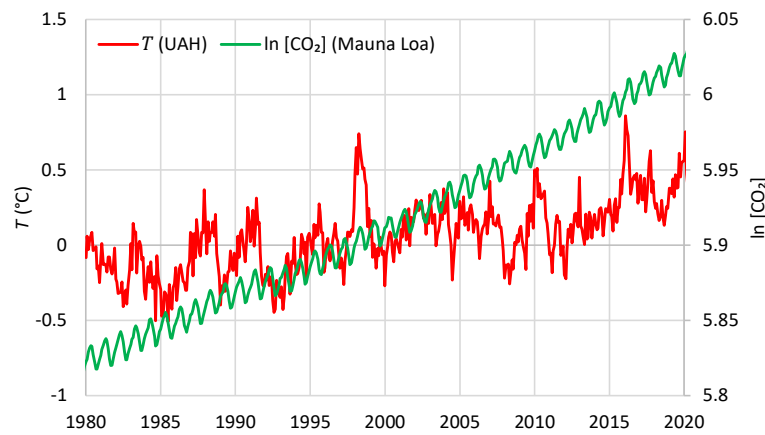


Figure 8. Synchronous plots of the time series of UAH temperature and logarithm of CO₂ concentration at Mauna Loa at monthly scale.

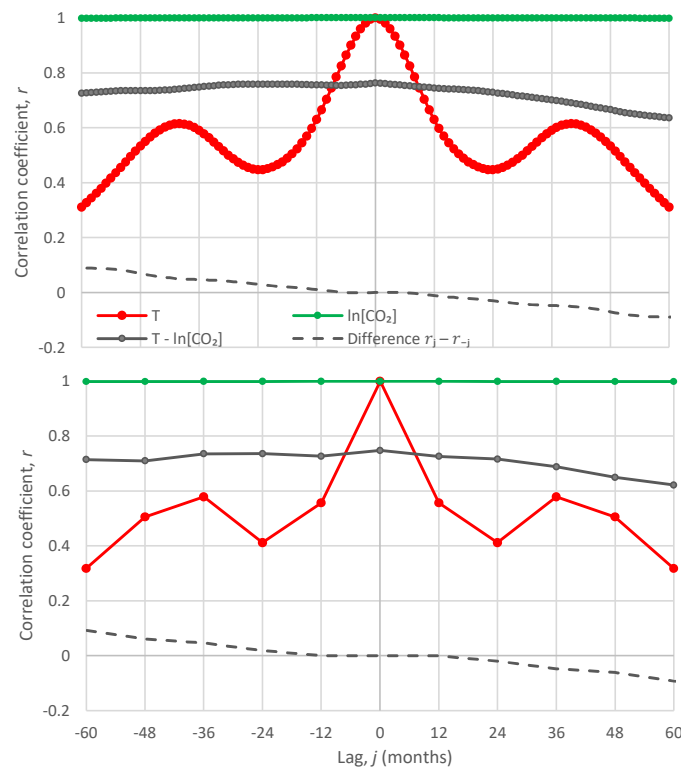


Figure 9. Auto- and cross-correlograms of the time series of UAH temperature and logarithm of CO₂ concentration at Mauna Loa.

In our investigation we also applied the Granger test on these two time series in both time directions. To calculate the p -value of the Granger test we used free software (namely the function GRANGER_TEST [52,53]). It appears that in the causality direction $[CO_2] \rightarrow T$ the null hypothesis is rejected at all usual significance levels. The attained p -value of the test is 1.8×10^{-7} for one regression lag ($\eta = 1$), 1.8×10^{-4} for $\eta = 2$ and keeps being below 0.01 for subsequent η . In contrast, in the direction $T \rightarrow [CO_2]$ the null hypothesis is not rejected at all usual significance levels. The attained p -value of the test is 0.25 for $\eta = 1$, 0.22 for $\eta = 2$ and remains above 0.1 for subsequent η .

Therefore, one could directly interpret these results as unambiguously showing one-way causality between the total greenhouse gases and temperature, and hence validating the consensus view that human activity is responsible for the observed rise in global temperature. However, these results are

certainly not unambiguous and most probably they are spurious. To see that they are not unambiguous, we have plotted in the upper panels of Figure 10 the p -values of the Granger test for moving windows with a size of 10 years for number of lags $\eta = 1$ and 2. The values for the entire length of time series, as given above, are also shown as dashed lines. Now the picture is quite different: each of the two directions appear dominating (meaning that the attained significance level is lower in one over the other) in about equal portions of the time. For example, for $\eta = 2$ the $T \rightarrow [\text{CO}_2]$ dominates over $[\text{CO}_2] \rightarrow T$ for 58% of the time. The attained p -value for direction $T \rightarrow [\text{CO}_2]$ is lower than 1% for 1.4% of the time, much higher than in the opposite direction (0.3% of the time). All these favour the $T \rightarrow [\text{CO}_2]$ direction.

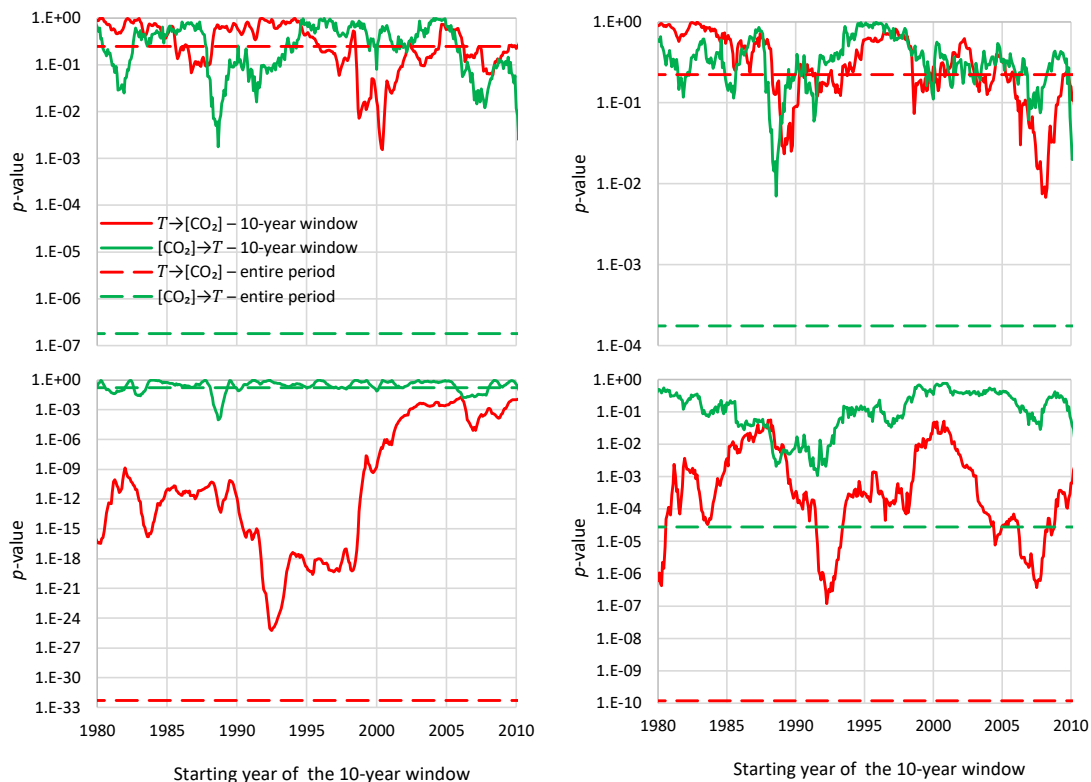


Figure 10. Plots of p -values of the Granger test for 10-year-long moving windows for the monthly time series of UAH temperature and logarithm of CO_2 concentration at Mauna Loa for number of lags (**left**) $\eta = 1$ and (**right**) $\eta = 2$. The time series used are: (**upper**) the original, and (**lower**) the obtained after “removing” the periodicity by averaging over the previous 12 months.

To show that the results are spurious and, in particular, affected by the very high autocorrelations of $\ln [\text{CO}_2]$ and, more importantly, by its annual cyclicity, we have “removed” the latter by averaging over the previous 12 months. We did that for both series and plotted the results in the lower panels of Figure 10. Here the results are stunning. For both lags $\eta = 1$ and 2 and for the entire period (or almost), the $T \rightarrow [\text{CO}_2]$ dominates, attaining p -values as low as in the order of 10^{-33} . However, we will avoid interpreting these results as unambiguous evidence that the consensus view (i.e., human activity is responsible for the observed warming) is wrong. Rather, what we want to stress is that a methodology which proves to be so sensitive to time windows used and data processing assumptions is inappropriate to draw conclusions from. In this respect, we have included this analyses in our study only: (a) to show its weaknesses (which, for the reasons we explained in Section 4.2 we not believe would change if we used different statistics or different time series) and (b) to connect our study to earlier ones. For the sake of drawing conclusions, we contend that our full methodology of Sections 4.1 and 4.3 is more appropriate. We apply this methodology in Section 5.2.

5.2. Differenced Time Series

We have already explained the advantages of investigating the differenced processes, which quantify changes, from a mathematical and logical point of view. In our case, taking differences is also physically meaningful as both CO₂ concentration and temperature (equivalent to thermal energy) represent “stocks”, i.e., stored quantities, and, thus, indeed the mass and energy fluxes are represented by differences.

The time step of differencing was chosen equal to one year ($\nu = 12$ for the monthly time step of the time series). For instance, from the value of January of a certain year we subtract the value of January of the previous year and so forth. A first reason for this choice is that it almost eliminates the effect of the annual cycle (periodicity). A second reason is that the temperature data are given in terms of “anomalies”, i.e., differences from an average which varies from month to month. By taking $\nu = 12$, the varying means are eliminated and “anomalies” are effectively replaced by the actual processes (as the differences in the actual values equal the differences of “anomalies”).

We perform all analyses on both monthly and annual time scales. Figure 11 shows the differenced time series for the UAH temperature and Mauna Loa CO₂ concentration at monthly scale; the symbols ΔT and $\Delta \ln[\text{CO}_2]$ are used interchangeably with $\tilde{x}_{\tau,12}$ and $\tilde{y}_{\tau,12}$, respectively.

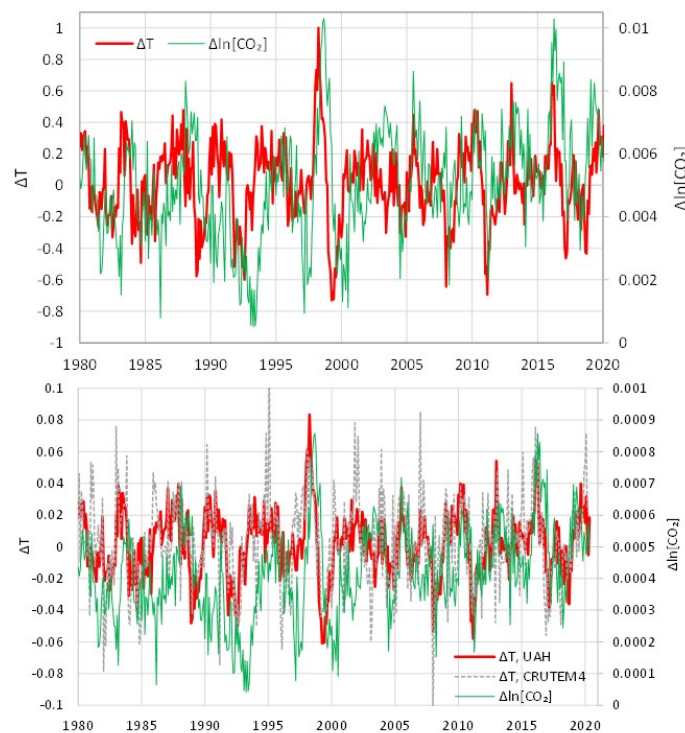


Figure 11. Differenced time series of UAH temperature and logarithm of CO₂ concentration at Mauna Loa at monthly scale. The graph in the upper panel was constructed in the manner described in the text. The graph in the lower panel is given for comparison and was constructed differently, by taking differences of the values of each month with the previous month and then averaging over the previous 12 months (to remove periodicity); in addition, the lower graph includes the CRUTEM4 land temperature series.

Comparing Figure 8 (undifferenced series) and Figure 11 (differenced series), one can verify that the latter is much more informative in terms of the directionality of the relationship of the two processes. While Figure 8 did not provide any relevant hint, Figure 11 clearly shows that most often the temperature curve leads and that of CO₂ follows. However, there are cases where the changes in the two processes synchronize in time or even become decoupled.

Figure 12 shows the same time series at the annual time scale, with the year being defined as July–June for ΔT and February–January for $\Delta \ln[\text{CO}_2]$. The reason for this differentiation will be explained below. Here it is more evident that most of the time the temperature change leads and that of CO_2 follows.

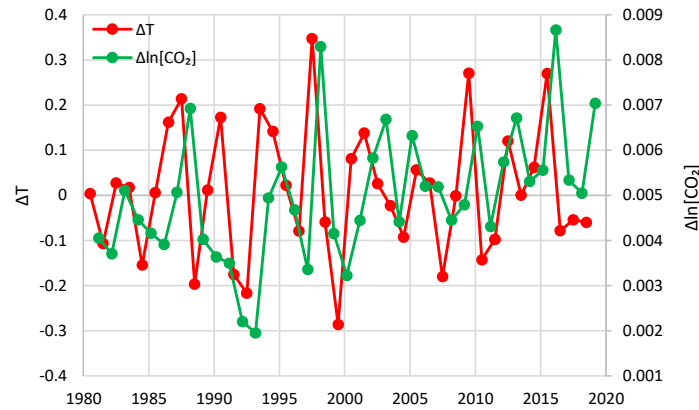


Figure 12. Annually averaged time series of differenced temperatures (UAH) and logarithms of CO_2 concentrations (Mauna Loa). Each dot represents the average of a one-year duration ending at the time of its abscissa.

It is of interest here that the variability of global mean annual temperature is significantly influenced by the rhythm of ocean-atmosphere oscillations, such as ENSO, AMO and IPO [54]. This mechanism may be a complicating factor, in turn influencing the link between temperature and CO_2 concentration. However, this is not examined further here as, given the focus in examining just the connection of the latter two processes, it lies out of our present scope.

The climacograms of the differenced time series used (actually four of the six to avoid an overcrowded graph) are shown in Figure 13. It appears that the differenced temperature time series are consistent with the condition implied by stationarity, i.e., $H = 0$ for the differenced process. The same does not look to be the case for the CO_2 time series, particularly for the Mauna Loa time series, in which the Hurst parameter appears to be close to $1/2$. Based on this, one would exclude stationarity for the Mauna Loa CO_2 time series. However, a simpler interpretation of the graph is that the data record is not long enough to reveal that $H = 0$ for the differenced process. Actually, all available data belong to a period in which $[\text{CO}_2]$ exhibits a monotonic increasing trend (as also verified by the fact that all values of $\Delta \ln[\text{CO}_2]$ in Figures 11 and 12 are positive, while stationarity entails a zero mean of the differenced process). Had the available data base been broader, both positive and negative trends could appear. Indeed, a broader view of the $[\text{CO}_2]$ process, based on palaeoclimatic data (Figures 3 and 4) would justify a stationarity assumption.

The preliminary qualitative observation from graphical inspection of Figures 11 and 12 suggests that the temperature change very often precedes and the CO_2 change follows—in the same direction. We note, though, that temperature changes alternate in sign while CO_2 changes are always positive.

A quantitative analysis, based on the methodology in Section 4.1 requires the study of lagged cross-correlations of the two processes. Figure 14 shows the cross-correlogram between UAH temperature and Mauna Loa CO_2 concentration; the autocorrelograms of the two processes are also plotted for comparison. The fact that the cross-correlogram does not have values consistently close to zero at any of the semi-axes eliminates the possibility of an exclusive (unidirectional) causality and suggests consistency with “hen-or-egg” causality.

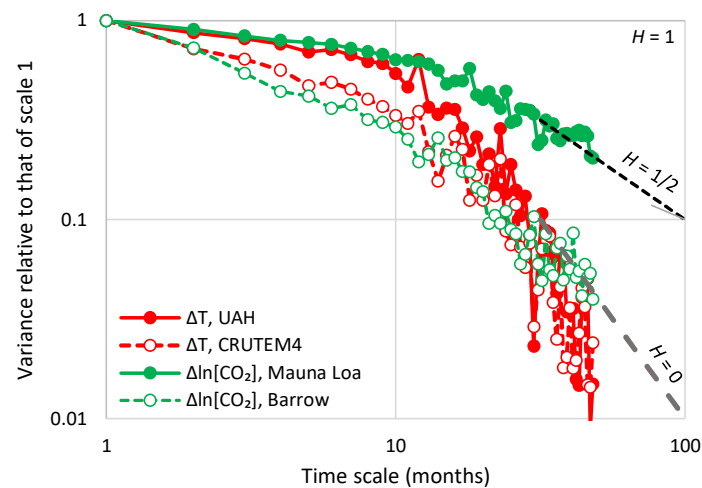


Figure 13. Empirical climacograms of the indicated differenced time series; the characteristic slopes corresponding to values of the Hurst parameter $H = 1/2$ (large-scale randomness), 0 (full antipersistence) and 1 (full persistence) are also plotted (note, $H = 1 + \text{slope}/2$).

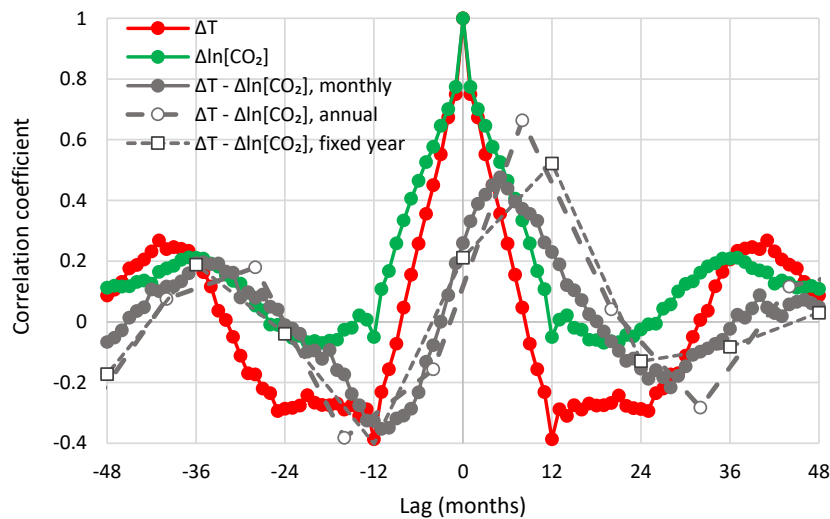


Figure 14. Auto- and cross-correlograms of the differenced time series of UAH temperature and Mauna Loa CO_2 concentration.

The maximum cross correlation of the monthly series is 0.47 and appears at a positive lag, $\eta_1 = 5$ months, thus suggesting $T \rightarrow [\text{CO}_2]$, rather than $[\text{CO}_2] \rightarrow T$, as dominant causality direction. Similar are the graphs of the other combinations of temperature and CO_2 datasets, which are shown in Appendix A.3 (Figures A3–A7). In all cases η_1 is positive, ranging from 5 to 11 months.

To perform similar analyses on the annual scale, we fixed the specification of a year for temperature for the period July–June, as already mentioned, and then slid the initial month specifying the beginning of a year for CO_2 concentration so as to find a specification that maximizes the cross-correlation at the annual scale. In Figure 14, maximization occurs when the year specification is February–January (of the next year), i.e., if the lag is 8 months. The maximum cross-correlation is 0.66. If we keep the specification of the year for CO_2 concentration the same as in temperature (July–June), then maximization occurs at lag one year (12 months) and the maximum cross correlation is 0.52. Table 1 summarizes the results for all combinations examined. The lags are always positive. They vary between 8 and 14 months for a sliding window specification and are 12 months, for the fixed window specification. Most interestingly, the opposite phase in the annual cycle of CO_2 concentration in the South Pole, with respect to the other

three sites, does not produce any noteworthy difference in the shape of the cross-correlogram and the time lags maximizing the cross-correlations.

Table 1. Maximum cross-correlation coefficient (MCCC) and corresponding time lag in months. The annual window for temperature is July–June, while for CO₂ it is either different (sliding), determined so as to maximize MCCC, or the same (fixed).

Temperature—CO ₂ Series	Monthly Time Series		Annual Time Series—Sliding Annual Window		Annual Time Series—Fixed Annual Window	
	MCCC	Lag	MCCC	Lag	MCCC	Lag
UAH—Mauna Loa	0.47	5	0.66	8	0.52	12
UAH—Barrow	0.31	11	0.70	14	0.59	12
UAH—South Pole	0.37	6	0.54	10	0.38	12
UAH—Global	0.47	6	0.60	11	0.60	12
CRUTEM4—Mauna Loa	0.31	5	0.55	10	0.52	12
CRUTEM4—Global	0.33	9	0.55	12	0.55	12

While, as explained in Sections 4.2 and 5.1, the Granger test has weaknesses that may not help in drawing conclusions, for completeness and as a confirmation we list here its results:

- For the monthly scale and the causality direction [CO₂] → T, the null hypothesis is not rejected at all usual significance levels for η = 1 and is rejected for significance level 1% for η = 2–8, with minimum attained p-value 1.4 × 10⁻⁴ for η = 6.
- For the monthly scale and the causality direction T → [CO₂], the null hypothesis is rejected at all usual significance levels for all η, with minimum attained p-value 1.4 × 10⁻⁸ for η = 6.
- For the monthly scale the attained p-values in the direction T → [CO₂] are always smaller than in direction [CO₂] → T by about 4 to 5 orders of magnitude, thus clearly supporting T → [CO₂] as dominant direction.
- For the annual scale with fixed year specification and the causality direction [CO₂] → T, the null hypothesis is not rejected at all usual significance levels for any η, thus indicating that this causality direction does not exist.
- For the annual scale with fixed year specification and the causality direction T → [CO₂], the null hypothesis is rejected at significance level 1% for all η = 1–6, with minimum attained p-value 0.05% for η = 2, thus supporting this causality direction.
- For the annual scale with fixed year specification the attained p-values in the direction T → [CO₂] are always smaller than in direction [CO₂] → T by about 1 to 3 orders of magnitude, again clearly supporting T → [CO₂] as the dominant direction.

We note that the test cannot be applied for the sliding time window case, and hence we cannot provide results for this case.

In brief, all above confirm the results of our methodology that the dominant direction of causality is T → [CO₂].

6. Physical Interpretation

The omnipresence of positive lags on both monthly and annual time scales and the confirmation by Granger tests reduce the likelihood that our results are statistical artefacts. Still, our results require physical interpretation which we seek in the natural process of soil respiration.

Soil respiration, R_s, defined to be the flux of microbially and plant-respired CO₂, clearly increases with temperature. It is known to have increased in the recent years [55,56]. Observational data of R_s (e.g., [57]) show that the process intensity increases with temperature. Rate of chemical reactions, metabolic rate, as well as microorganism activity, generally increase with temperature. This has been known for more than 70 years (Pomeroy and Bowlus [58]) and is routinely used in engineering design.

The latest report of the IPCC [56] (Figure 6.1) gives quantification of the mass balance of the carbon cycle in the atmosphere, representative of the recent years. The soil respiration, assumed to be the sum

of respiration (plants) and decay (microbes) is 113.7 Gt C/year (IPCC gives a value of 118.7 including fire, which, along with biomass burning, is estimated to 5 Gt C/year by Green and Byrne [59]).

We can expect that sea respiration would have increased, too. Also, photosynthesis must have been increased as in the 21st century the Earth has been greening, mostly due to CO₂ fertilization effects [60] and human land-use management [61]. Specifically, satellite data show a net increase in leaf area of 2.3% per decade [61]. The sums of carbon outflows from the atmosphere (terrestrial and maritime photosynthesis as well as maritime absorption) amount to 203 Gt C/year. The carbon inflows to the atmosphere amount to 207.4 Gt C/year and include natural terrestrial processes (respiration, decay, fire, freshwater outgassing as well as volcanism and weathering), natural maritime processes (respiration) as well as anthropogenic processes. The latter comprise human CO₂ emissions related to fossil fuels and cement production as well as land-use change, and amount to 7.7 Gt C/year and 1.1 Gt C/year, respectively. The change in carbon fluxes due to natural processes is likely to exceed the change due to anthropogenic CO₂ emissions, even though the latter are generally regarded as responsible for the imbalance of carbon in the atmosphere.

7. Conclusions

The relationship between atmospheric concentration of carbon dioxide and the global temperature is widely recognized and it is common knowledge that increasing CO₂ concentration plays a major role in enhancement of the greenhouse effect and contributes to global warming.

While the fact that these two variables are tightly connected is beyond doubt, the direction of the causal relationship needs to be studied further. The purpose of this study is to complement the conventional and established theory that increased CO₂ concentration due to anthropogenic emissions causes an increase of temperature, by considering the concept of reverse causality. The problem is obviously more complex than that of exclusive roles of cause and effect, qualifying as a “hen-or-egg” (“ὄρνις ἢ ᾠδόν”) causality problem, where it is not always clear which of two interrelated events is the cause and which the effect. Increased temperature causes an increase in CO₂ concentration and hence we propose the formulation of the entire process in terms of a “hen-or-egg” causality.

We examine the relationship of global temperature and atmospheric carbon dioxide concentration using the most reliable global data that are available—the data gathered from several sources, covering the common time interval 1980–2019, available at the monthly time step.

The results of the study support the hypothesis that both causality directions exist, with $T \rightarrow \text{CO}_2$ being the dominant, despite the fact that the former $\text{CO}_2 \rightarrow T$ prevails in public, as well as in scientific perception. Indeed, our results show that changes in CO₂ follow changes in T by about six months on a monthly scale, or about one year on an annual scale.

The opposite causality direction opens a nurturing interpretation question. We attempted to interpret this mechanism by noting that the increase of soil respiration, reflecting the fact that the intensity of biochemical process increases with temperature, leads to increasing natural CO₂ emission. Thus, the synchrony of rising temperature and CO₂ creates a positive feedback loop. This poses challenging scientific questions of interpretation and modelling for further studies. In our opinion, scientists of the 21st century should have been familiar with unanswered scientific questions, as well as with the idea that complex systems resist simplistic explanations.

Author Contributions: Conceptualization, D.K.; methodology, D.K.; software, D.K.; validation, Z.W.K.; formal analysis, D.K.; investigation, D.K. and Z.W.K.; data curation, D.K.; writing—original draft preparation, D.K. and Z.W.K.; writing—review and editing, D.K. and Z.W.K.; visualization, D.K. and Z.W.K. All authors have read and agreed to the published version of the manuscript.

Funding: This research received no external funding but was motivated by the scientific curiosity of the authors.

Acknowledgments: Some negative comments of two anonymous reviewers of an earlier submission of this manuscript in another journal (which we have posted online: manuscript at <http://dx.doi.org/10.13140/RG.2.2.29154.15045/1>, reviews at <http://dx.doi.org/10.13140/RG.2.2.14524.87681>) helped us improve the presentation and strengthen our arguments against their comments. We appreciate these reviewers’ suggestions of relevant published works, which we were unaware of.

Conflicts of Interest: The authors declare no conflict of interest.

Data Availability: The two temperature time series and the Mauna Loa CO₂ time series are readily available on monthly scale from <http://climexp.knmi.nl>. All NOAA CO₂ data are available from https://www.esrl.noaa.gov/gmd/ccgg/trends/gl_trend.html. The CO₂ data of Mauna Loa were retrieved from http://climexp.knmi.nl/data/imaunaloa_f.dat while the original measurements are in <https://www.esrl.noaa.gov/gmd/dv/iadv/graph.php?code=MLO>. The Barrow series is available (in irregular step) in <https://www.esrl.noaa.gov/gmd/dv/iadv/graph.php?code=BRW>, and the South Pole series in <https://www.esrl.noaa.gov/gmd/dv/data/index.php?site=SPO>. All these data were accessed (using the “Download data” link in the above sites) in June 2020. The global CO₂ series is accessed at https://www.esrl.noaa.gov/gmd/ccgg/trends/gl_data.html, of which the “Globally averaged marine surface monthly mean data” are used here. The palaeoclimatic data of Vostok CO₂ were retrieved from <http://cdiac.ess-dive.lbl.gov/ftp/trends/co2/vostok.icecore.co2> (dated January 2003, accessed September 2018) and the temperature data from <http://cdiac.ess-dive.lbl.gov/ftp/trends/temp/vostok/vostok.1999.temp.dat> (dated January 2000, accessed September 2018).

Appendix A

Appendix A.1. Some Notes on the Averaged Differenced Process

The cumulative process of the differenced process $\tilde{x}_{\tau,\nu}$ will be:

$$\tilde{X}_{\kappa,\nu} := \tilde{x}_{1,\nu} + \tilde{x}_{2,\nu} + \dots + \tilde{x}_{\kappa,\nu} = x_{1+\nu} - x_1 + x_{2+\eta} - x_2 + \dots + x_{\kappa+\nu} - x_\kappa = X_{\kappa+\nu} - X_\nu - X_\kappa \tag{A1}$$

Note that for $\eta = 1$ this simplifies to:

$$\tilde{X}_{\kappa,1} = X_{\kappa+1} - X_1 - X_\kappa = x_{\kappa+1} - x_1 = \tilde{x}_{\kappa,1} := \tilde{x}_\kappa \tag{A2}$$

Following Equation (7), the average differenced process at discrete time scale $\kappa = \eta$ will be:

$$\tilde{x}_\tau^{(\kappa)} = \frac{\tilde{X}_{\tau\kappa,\kappa} - \tilde{X}_{(\tau-1)\kappa,\kappa}}{\kappa} = \frac{(X_{\tau\kappa+\kappa} - X_\kappa - X_{\tau\kappa}) - (X_{(\tau-1)\kappa+\kappa} - X_\kappa - X_{(\tau-1)\kappa})}{\kappa} \tag{A3}$$

which, noting that in the rightmost part the two terms X_κ cancel each other and by virtue of (7), simplifies to:

$$\tilde{x}_\tau^{(\kappa)} = x_{\tau+1}^{(\kappa)} - x_\tau^{(\kappa)} = \tilde{x}_{\tau,1}^{(\kappa)} \tag{A4}$$

In other words, the average differenced process equals the differenced average process in case that the differencing time step η has chosen equal to the averaging time scale κ . For $\kappa = \eta = 1$ we have $\tilde{x}_\tau^{(1)} \equiv \tilde{x}_{\tau,1} \equiv \tilde{x}_\tau$.

Appendix A.2. Some Notes on Time Directionality of Causal Systems

In a unidirectional causal system in continuous time t , in which the process $\underline{x}(t)$ is the cause of $\underline{y}(t)$, an equation of the form:

$$\underline{y}(t) = \int_0^\infty \alpha(s)\underline{x}(t-s)ds \tag{A5}$$

should hold [49], where $\alpha(t)$ is the impulse response function. The causality condition is thus:

$$\alpha(t) = 0 \text{ for } t < 0 \tag{A6}$$

Here we consider systems with positive dependence, in which $\alpha(t) \geq 0$ for $t \geq 0$, which possibly are also excited by another process $\underline{v}(t)$, independent of $\underline{x}(t)$. Working in discrete time we write:

$$\underline{y}_\tau = \sum_{j=0}^\infty \alpha_j \underline{x}_{\tau-j} + \underline{v}_\tau \tag{A7}$$

Assuming (without loss of generality) zero means for all processes, multiplying by $\underline{x}_{t-\eta}$, taking expected values and denoting the cross-covariance function as $c_{xy}[\eta] := E\left[\underline{x}_{t-\eta}\underline{y}_t\right]$ and the autocovariance function as $c_x[\eta] := E\left[\underline{x}_{t-\eta}\underline{x}_t\right]$ we find:

$$c_{xy}[\eta] = \sum_{j=0}^{\infty} \alpha_j c_x[\eta - j] \tag{A8}$$

For $\eta > 0$, using the property that $c_x[\eta]$ is an even function ($c_x[\eta] = c_x[-\eta]$) we get:

$$c_{xy}[\eta] = \sum_{j=0}^{\infty} \alpha_j c_x[j - \eta] = \sum_{j=0}^{\eta-1} \alpha_j c_x[\eta - j] + \sum_{j=\eta}^{\infty} \alpha_j c_x[j - \eta] \tag{A9}$$

and for the negative part:

$$c_{xy}[-\eta] = \sum_{j=0}^{\infty} \alpha_j c_x[j + \eta] \tag{A10}$$

With intuitive reasoning, assuming that the autocovariance function is decreasing ($c_x[j'] < c_x[j]$ for $j' > j$), as usually happens in natural processes, we may see that the rightmost term of Equations (A9) and (A10) should be decreasing functions of η (as for $j' > j$ it will be $c_x[j' - \eta] < c_x[j - \eta]$ and $c_x[j' + \eta] < c_x[j + \eta]$). However, the term $\sum_{j=0}^{\eta-1} \alpha_j c_x[\eta - j]$ of Equation (A9), is not decreasing. Therefore, it should attain a maximum value at some positive lag $\eta = \eta_1$. Thus, a positive maximizing lag, $\eta = \eta_1 > 0$, is a necessary condition for causality direction from \underline{x}_t to \underline{y}_t . Conversely, the condition that the maximizing lag is negative is a sufficient condition to exclude the causality direction exclusively from \underline{x}_t to \underline{y}_t .

All above arguments remain valid if we standardize (divide) by the product of standard deviations of the processes \underline{x}_t and \underline{y}_t , and thus we can replace cross-covariances $c_{xy}[\eta]$ with cross-correlations $r_{xy}[\eta]$ (or, in the case of differenced processes, $r_{xy}[\nu, \eta]$).

Appendix A.3. Additional Graphical Depictions

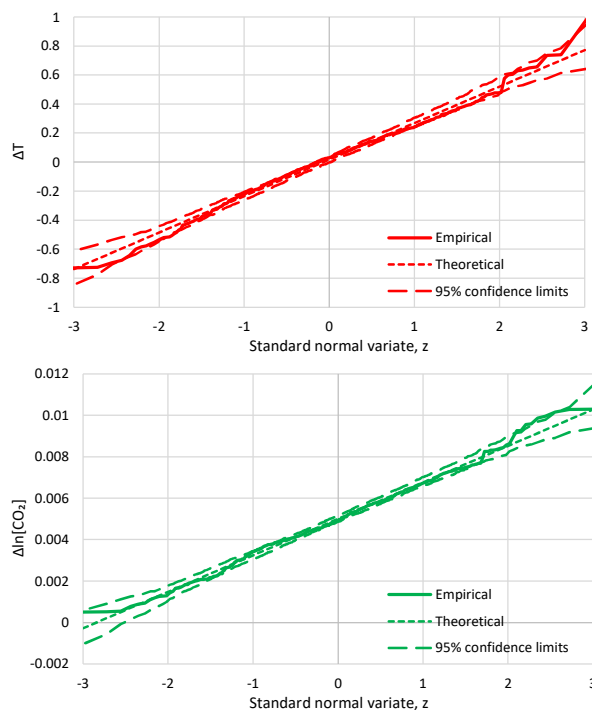


Figure A1. Normal probability plots of ΔT and $\Delta \ln[\text{CO}_2]$ where T is the UAH temperature and $[\text{CO}_2]$ is the CO_2 concentration at Mauna Loa at monthly scale.

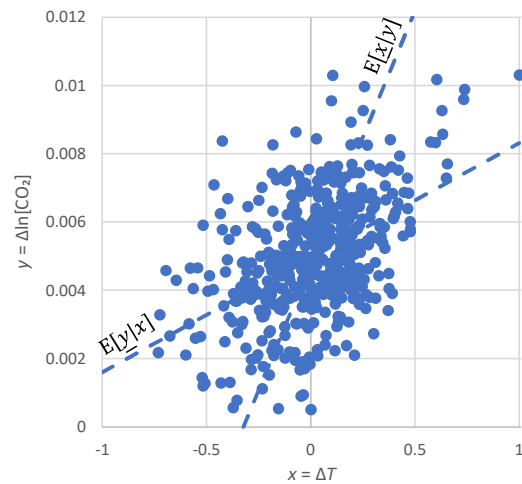


Figure A2. Scatter plot of ΔT and $\Delta \ln [\text{CO}_2]$ where T is the UAH temperature and $[\text{CO}_2]$ is the CO_2 concentration at Mauna Loa at monthly scale; the two quantities are lagged in time using the optimal the lag of 5 months (Table 1). The two linear regression lines are also shown in the figure.

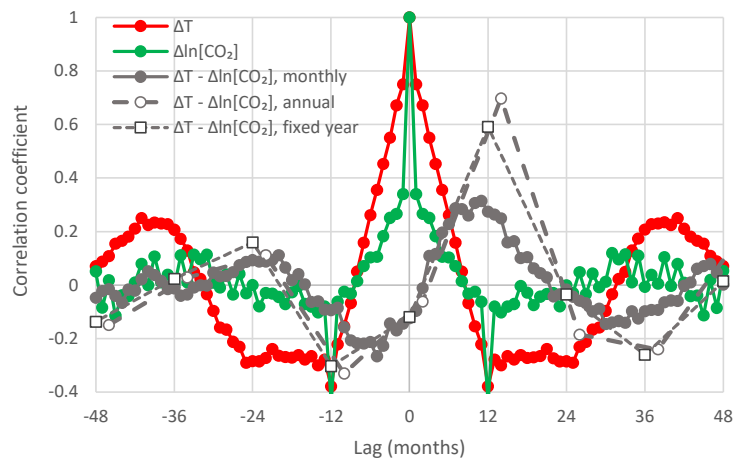


Figure A3. Auto- and cross-correlograms of the differenced time series of UAH temperature and Barrow CO_2 concentration.

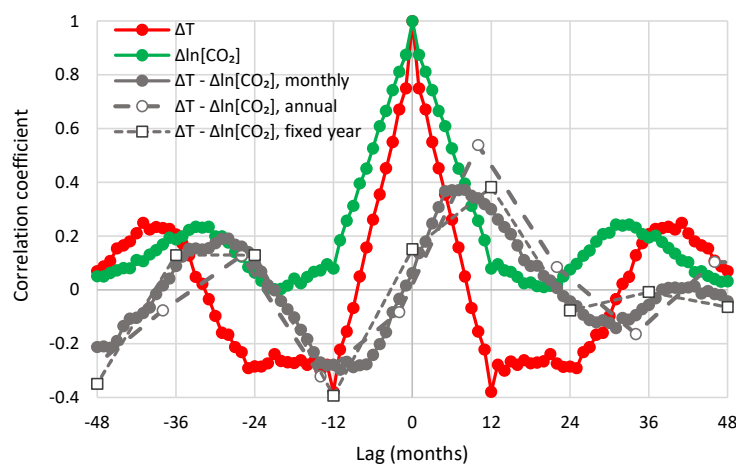


Figure A4. Auto- and cross-correlograms of the differenced time series of UAH temperature and South Pole CO_2 concentration.

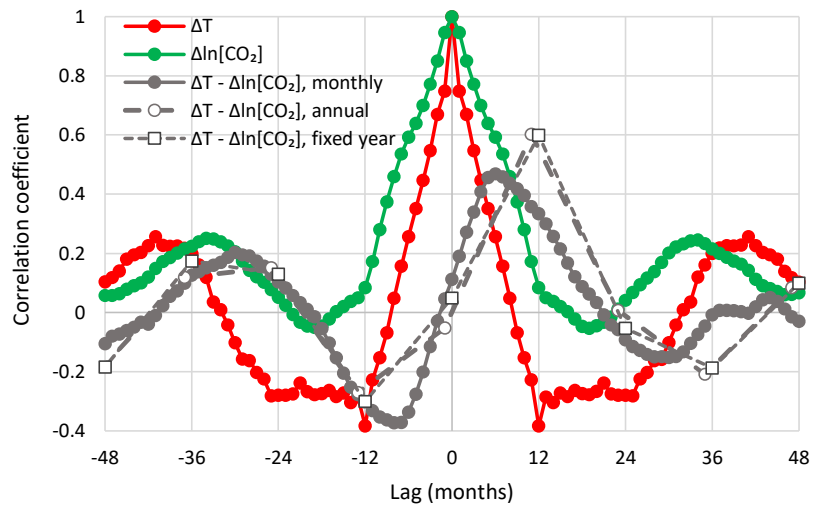


Figure A5. Auto- and cross-correlograms of the differenced time series of UAH temperature and global CO₂ concentration.

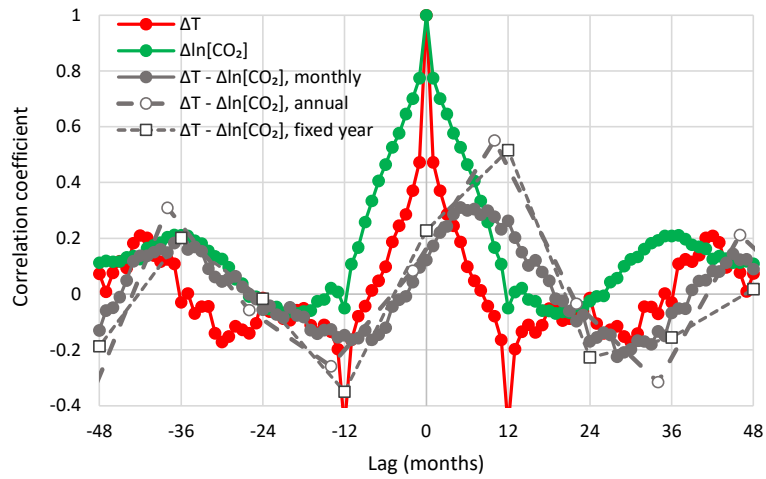


Figure A6. Auto- and cross-correlograms of the differenced time series of CRUTEM4 temperature and Mauna Loa CO₂ concentration.

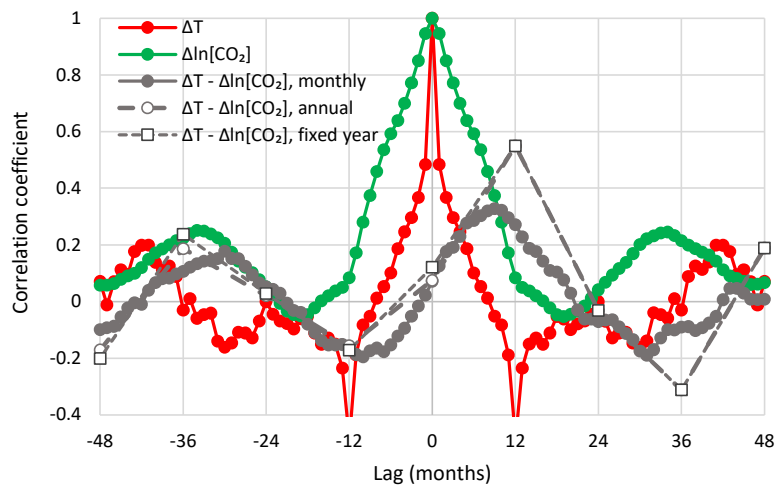


Figure A7. Auto- and cross-correlograms of the differenced time series of CRUTEM4 temperature and global CO₂ concentration.

References

1. IEA (International Energy Agency). *Global Energy Review 2020*; IEA: Paris, French, 2020. Available online: <https://www.iea.org/reports/global-energy-review-2020> (accessed on 1 July 2020).
2. Le Quéré, C.; Jackson, R.B.; Jones, M.W.; Smith, A.J.; Abernethy, S.; Andrew, R.M.; De-Gol, A.J.; Willis, D.R.; Shan, Y.; Canadell, J.G.; et al. Temporary reduction in daily global CO₂ emissions during the COVID-19 forced confinement. *Nat. Clim. Chang.* **2020**, *10*, 647–653. [[CrossRef](#)]
3. Peters, G.P.; Marland, G.; Le Quéré, C.; Boden, T.; Canadell, J.G.; Raupach, M.R. Rapid growth in CO₂ emissions after the 2008–2009 global financial crisis. *Nat. Clim. Chang.* **2012**, *2*, 2–4. [[CrossRef](#)]
4. Arrhenius, S. On the influence of carbonic acid in the air upon the temperature of the ground. *Lond. Edinb. Dublin Philos. Mag. J. Sci.* **1896**, *41*, 237–276. [[CrossRef](#)]
5. De Marchi, L. *Le Cause dell’Era Glaciale*; Premiato dal R. Istituto Lombardo: Pavia, Italy, 1895.
6. Tyndall, J. *Heat a Mode of Motion*, 2nd ed.; Longmans: London, UK, 1865. Available online: <https://archive.org/details/heatamodemotion05tyndgoog/> (accessed on 1 September 2020).
7. Foote, E. Circumstances affecting the heat of the sun’s rays. *Am. J. Sci. Arts* **1856**, *22*, 382–383.
8. Jackson, R. Eunice Foote, John Tyndall and a question of priority. *Notes Rec.* **2020**, *74*, 105–118. [[CrossRef](#)]
9. Ortiz, J.D.; Jackson, R. Understanding Eunice Foote’s 1856 experiments: Heat absorption by atmospheric gases. *Notes Rec.* **2020**. [[CrossRef](#)]
10. Schmidt, G.A.; Ruedy, R.A.; Miller, R.L.; Lacis, A.A. Attribution of the present-day total greenhouse effect. *J. Geophys. Res.* **2010**, *115*, D20106. [[CrossRef](#)]
11. Roe, G. In defense of Milankovitch. *Geophys. Res. Lett.* **2006**, *33*. [[CrossRef](#)]
12. Jouzel, J.; Lorius, C.; Petit, J.R.; Genthon, C.; Barkov, N.I.; Kotlyakov, V.M.; Petrov, V.M. Vostok ice core: A continuous isotope temperature record over the last climatic cycle (160,000 years). *Nature* **1987**, *329*, 403–408. [[CrossRef](#)]
13. Petit, J.R.; Jouzel, J.; Raynaud, D.; Barkov, N.I.; Barnola, J.-M.; Basile, I.; Bender, M.; Chappellaz, J.; Davis, M.; Delayque, G.; et al. Climate and atmospheric history of the past 420,000 years from the Vostok ice core, Antarctica. *Nature* **1999**, *399*, 429–436. [[CrossRef](#)]
14. Caillon, N.; Severinghaus, J.P.; Jouzel, J.; Barnola, J.M.; Kang, J.; Lipenkov, V.Y. Timing of atmospheric CO₂ and Antarctic temperature changes across Termination III. *Science* **2003**, *299*, 1728–1731. [[CrossRef](#)] [[PubMed](#)]
15. Soon, W. Implications of the secondary role of carbon dioxide and methane forcing in climate change: Past, present, and future. *Phys. Geogr.* **2007**, *28*, 97–125. [[CrossRef](#)]
16. Pedro, J.B.; Rasmussen, S.O.; van Ommen, T.D. Tightened constraints on the time-lag between Antarctic temperature and CO₂ during the last deglaciation. *Clim. Past* **2012**, *8*, 1213–1221. [[CrossRef](#)]
17. Koutsoyiannis, D. Time’s arrow in stochastic characterization and simulation of atmospheric and hydrological processes. *Hydrol. Sci. J.* **2019**, *64*, 1013–1037. [[CrossRef](#)]
18. Chowdhry Beeman, J.; Gest, L.; Parrenin, F.; Raynaud, D.; Fudge, T.J.; Buizert, C.; Brook, E.J. Antarctic temperature and CO₂: Near-synchrony yet variable phasing during the last deglaciation. *Clim. Past* **2019**, *15*, 913–926. [[CrossRef](#)]
19. Scotese, C.R. Phanerozoic Temperatures: Tropical Mean Annual Temperature (TMAT), Polar Mean Annual Temperature (PMAT), and Global Mean Annual Temperature (GMAT) for the last 540 Million Years. Earth’s Temperature History Research Workshop, Smithsonian National Museum of Natural History, 30–31 March 2018, Washington, D.C. Available online: <https://www.researchgate.net/publication/324017003> (accessed on 8 September 2020).
20. Royer, D.L.; Berner, R.A.; Montañez, I.P.; Tabor, N.J.; Beerling, D.J. CO₂ as a primary driver of Phanerozoic climate. *GSA Today* **2004**, *14*, 4–10. [[CrossRef](#)]
21. Grossman, E.L. Oxygen isotope stratigraphy. In *The Geological Time Scale*; Gradstein, F.M., Ogg, J.G., Schmitz, M.D., Ogg, G.M., Eds.; Elsevier: Amsterdam, The Netherlands, 2012; pp. 181–206.
22. Veizer, J.; Prokoph, A. Temperatures and oxygen isotopic composition of Phanerozoic oceans. *Earth Sci. Rev.* **2015**, *146*, 92–104. [[CrossRef](#)]
23. Davis, W.J. The relationship between atmospheric carbon dioxide concentration and global temperature for the last 425 million years. *Climate* **2017**, *5*, 76. [[CrossRef](#)]
24. Berner, R.A. Addendum to “Inclusion of the weathering of volcanic rocks in the GEOCARBSULF model” (R. A. Berner, 2006, v. 306, p. 295–302). *Am. J. Sci.* **2008**, *308*, 100–103. [[CrossRef](#)]

25. Ekart, D.D.; Cerling, T.E.; Montanez, I.P.; Tabor, N.J. A 400 million year carbon isotope record of pedogenic carbonate: Implications for paleoatmospheric carbon dioxide. *Am. J. Sci.* **1999**, *299*, 805–827. [[CrossRef](#)]
26. Kodra, E.; Chatterjee, S.; Ganguly, A.R. Exploring Granger causality between global average observed time series of carbon dioxide and temperature. *Theor. Appl. Climatol.* **2011**, *104*, 325–335. [[CrossRef](#)]
27. Stern, D.I.; Kaufmann, R.K. Anthropogenic and natural causes of climate change. *Clim. Chang.* **2014**, *122*, 257–269. [[CrossRef](#)]
28. Stips, A.; Macias, D.; Coughlan, C.; Garcia-Gorrioz, E.; Liang, X.S. On the causal structure between CO₂ and global temperature. *Sci. Rep.* **2016**, *6*, 21691. [[CrossRef](#)] [[PubMed](#)]
29. Liang, X.S. Information flow and causality as rigorous notions ab initio. *Phys. Rev. E* **2016**, *94*, 052201. [[CrossRef](#)] [[PubMed](#)]
30. Spencer, R.W.; Christy, J.R. Precise monitoring of global temperature trends from satellites. *Science* **1990**, *247*, 1558–1562. [[CrossRef](#)]
31. Christy, J.R.; Norris, W.B.; Spencer, R.W.; Hnilo, J.J. Tropospheric temperature change since 1979 from tropical radiosonde and satellite measurements. *J. Geophys. Res.* **2007**, *112*, D06102. [[CrossRef](#)]
32. Jones, P.D.; Lister, D.H.; Osborn, T.J.; Harpham, C.; Salmon, M.; Morice, C.P. Hemispheric and large-scale land surface air temperature variations: An extensive revision and an update to 2010. *J. Geophys. Res.* **2012**, *117*, D05127. [[CrossRef](#)]
33. Koutsoyiannis, D. Revisiting global hydrological cycle: Is it intensifying? *Hydrol. Earth Syst. Sci.* **2020**. [[CrossRef](#)]
34. Keeling, C.D.; Bacastow, R.B.; Bainbridge, A.E.; Ekdahl, C.A.; Guenther, P.R.; Waterman, L.S. Atmospheric carbon dioxide variations at Mauna Loa observatory, Hawaii. *Tellus* **1976**, *28*, 538–551.
35. Lawrance, A.J. Directionality and reversibility in time series. *Int. Stat. Rev.* **1991**, *59*, 67–79. [[CrossRef](#)]
36. Weiss, G. Time-reversibility of linear stochastic processes. *J. Appl. Probab.* **1975**, *12*, 831–836. [[CrossRef](#)]
37. Tong, H.; Zhang, Z. On time-reversibility of multivariate linear processes. *Stat. Sin.* **2005**, *15*, 495–504.
38. Koutsoyiannis, D. Generic and parsimonious stochastic modelling for hydrology and beyond. *Hydrol. Sci. J.* **2016**, *61*, 225–244. [[CrossRef](#)]
39. Kolmogorov, A.N. Wiener'sche spiralen und einige andere interessante Kurven im Hilbertschen Raum. *Dokl. Akad. Nauk SSSR* **1940**, *26*, 115–118.
40. Hurst, H.E. Long term storage capacities of reservoirs. *Trans. Am. Soc. Civil Eng.* **1951**, *116*, 776–808.
41. Heller, M. Time, causality, and the quantum theory. *Rev. Metaphys.* **1983**, *37*, 408–409.
42. Kline, A.D. Are there cases of simultaneous causation? *PSA Proc. Bienn. Meet. Philos. Sci. Assoc.* **1980**, *1980*, 292–301, Philosophy of Science Association. [[CrossRef](#)]
43. Suppes, P. *A Probabilistic Theory of Causality*; North-Holland Publishing: Amsterdam, The Netherlands, 1970.
44. Granger, C.W. Testing for causality: A personal viewpoint. *J. Econ. Dyn. Control* **1980**, *2*, 329–352. [[CrossRef](#)]
45. Granger, C.; Newbold, P. *Forecasting Economic Time Series*; Academic Press: San Diego, CA, USA, 1986.
46. Gujarati, D.N.; Porter, D.C. *Basic Econometrics*, 5th ed.; McGraw Hill: Boston, MA, USA, 2009.
47. McGraw, M.C.; Barnes, E.A. Memory matters: A case for Granger causality in climate variability studies. *J. Clim.* **2018**, *31*, 3289–3300. [[CrossRef](#)]
48. Cohen, M.X. *Analyzing Neural Time Series Data: Theory and Practice*; MIT Press: Cambridge, MA, USA, 2014.
49. Papoulis, A. *Probability, Random Variables and Stochastic Processes*, 3rd ed.; McGraw-Hill: New York, NY, USA, 1991.
50. Paluš, M.; Krakovská, A.; Jakubík, J.; Chvosteková, M. Causality, dynamical systems and the arrow of time. *Chaos Interdiscip. J. Nonlinear Sci.* **2018**, *28*, 75307. [[CrossRef](#)]
51. Koutsoyiannis, D.; Yao, H.; Georgakakos, A. Medium-range flow prediction for the Nile: A comparison of stochastic and deterministic methods. *Hydrol. Sci. J.* **2008**, *53*, 142–164. [[CrossRef](#)]
52. Zaiontz, C. Real Statistics Using Excel. Available online: <http://www.realstatistics.com/> (accessed on 1 September 2020).
53. Zaiontz, C. Real Statistics Examples Workbooks. Available online: <http://www.real-statistics.com/free-download/real-statistics-examples-workbook/> (accessed on 1 September 2020).
54. Kundzewicz, Z.W.; Pińskwar, I.; Koutsoyiannis, D. Variability of global mean annual temperature is significantly influenced by the rhythm of ocean-atmosphere oscillations. *Sci. Total Environ.* **2020**, *747*, 141256. [[CrossRef](#)] [[PubMed](#)]

55. Bond-Lamberty, B.; Thomson, A. Temperature-associated increases in the global soil respiration record. *Nature* **2010**, *464*, 579–582. [[CrossRef](#)]
56. IPCC. *Climate Change 2013: The Physical Science Basis. Contribution of Working Group I to the Fifth Assessment Report of the Intergovernmental Panel on Climate Change*; Cambridge University Press: Cambridge, UK; New York, NY, USA, 2013; p. 1535. Available online: <http://www.climatechange2013.org/report/> (accessed on 14 February 2020).
57. Makita, N.; Kosugi, Y.; Sakabe, A.; Kanazawa, A.; Ohkubo, S.; Tani, M. Seasonal and diurnal patterns of soil respiration in an evergreen coniferous forest: Evidence from six years of observation with automatic chambers. *PLoS ONE* **2018**, *13*, e0192622. [[CrossRef](#)] [[PubMed](#)]
58. Pomeroy, R.; Bowlus, F.D. Progress report on sulfide control research. *Sew. Work. J.* **1946**, *18*, 597–640.
59. Green, C.; Byrne, K.A. Biomass: Impact on carbon cycle and greenhouse gas emissions. In *Encyclopedia of Energy*; Cleveland, C.J., Ed.; Elsevier: Amsterdam, The Netherlands, 2004; pp. 223–236. [[CrossRef](#)]
60. Zhu, Z.; Piao, S.; Myneni, R.B.; Huang, M.; Zeng, Z.; Canadell, J.G.; Ciais, P.; Sitch, S.; Friedlingstein, P.; Arneeth, A.; et al. Greening of the earth and its drivers. *Nat. Clim. Chang.* **2016**, *6*, 791–795. [[CrossRef](#)]
61. Chen, C.; Park, T.; Wang, X.; Piao, S.; Xu, B.; Chaturvedi, R.K.; Fuchs, R.; Brovkin, V.; Ciais, P.; Fensholt, R.; et al. China and India lead in greening of the world through land-use management. *Nat. Sustain.* **2019**, *2*, 122–129. [[CrossRef](#)]



© 2020 by the authors. Licensee MDPI, Basel, Switzerland. This article is an open access article distributed under the terms and conditions of the Creative Commons Attribution (CC BY) license (<http://creativecommons.org/licenses/by/4.0/>).